

The geometrically-averaged density of states as a measure of localization

Yun Song, W. A. Atkinson, R. Wortis

*Department of Physics & Astronomy, Trent University,
1600 West Bank Dr., Peterborough ON, K9J 7B8, Canada*

(Dated: September 5, 2018)

Motivated by current interest in disordered systems of interacting electrons, the effectiveness of the geometrically averaged density of states, $\rho_g(\omega)$, as an order parameter for the Anderson transition is examined. In the context of finite-size systems we examine complications which arise from finite energy resolution. Furthermore we demonstrate that even in infinite systems a decline in $\rho_g(\omega)$ with increasing disorder strength is not uniquely associated with localization.

I. INTRODUCTION

Although disordered metallic systems have been studied extensively for many years, a reasonably complete theoretical understanding has only been developed for noninteracting particles,¹ and the effect of interactions in disordered media is an open and challenging problem.

In 1958, Anderson² proposed that noninteracting electrons may be localized by the interference of wavefunctions elastically scattered off of multiple impurities even in situations in which the electrons are classically unconfined. Extensive studies¹ since then have produced a clear picture of the Anderson transition. In $d = 3$ dimensions, and for sufficient disorder, single-particle wavefunctions at the band edges are localized, and decay exponentially on a scale referred to as the localization length, ξ . ξ is a function of energy, and diverges at the upper and lower mobility edges $\omega_{c\pm}$ which separate localized and extended states; states with energies $\omega > \omega_{c+}$ or $\omega < \omega_{c-}$ are localized, while states with $\omega_{c-} < \omega < \omega_{c+}$ are extended. The mobility edges move towards the band center as disorder is increased, and a metal-insulator transition occurs when either mobility edge crosses the Fermi level.

The question of how electron-electron interactions influence the interference effects responsible for Anderson localization has received much attention^{1,3,4} with calculations using mean field, diagrammatic perturbation and renormalization techniques. While much has been learned, a clear understanding of the strong interaction limit has not been achieved. Recently a number of approaches have been developed to use dynamical mean field theory (DMFT) methods to study the Mott-Anderson metal-insulator transition.^{5,6,7,8,9,10,11} In its original form DMFT is a local approximation in which a single site is embedded in an effective medium. The distinction from standard mean-field theory is that the on-site interaction is treated exactly, and the effective medium is chosen to approximate the effects of other interactions. One solves self-consistently for the local single-particle Green's function $G(\mathbf{r}, \mathbf{r}, z)$, where \mathbf{r} is a position and z a complex frequency.

DMFT captures the physics of the interaction-driven metal-insulator transition¹² (the Mott transition), but two significant challenges arise in its application to the

study of the Anderson transition. First, one must capture the subtle physics of localization within an effective medium theory and, second, one must extract information about nonlocal behavior from the local Green's function. The first problem has been the topic of recent work,^{5,6,7,8,9,10,11} while the focus of the current article is the second: What quantity calculable from the local Green's function is a practical measure of localization?

For numerical calculations on noninteracting-electron systems, a number of convenient measures exist: including the Thouless number,^{13,14} spectral statistics,¹⁵ and especially the inverse participation ratio^{14,16} (IPR). A key point, however, is that in the absence of electron-electron interactions the many-body wavefunction is a product of well-defined single particle eigenstates, and all of these methods rely on knowledge of these states. However, in interacting systems no such states exist.

A possible approach is suggested by the fact^{14,17} that for a system with localized states the local density of states (LDOS), $\rho(\mathbf{r}, \omega) = -\pi^{-1} \text{Im} G(\mathbf{r}, \mathbf{r}, \omega + i0^+)$, has a discrete spectrum. In an infinite system the density of states of the whole system (DOS) is in general a continuous function of ω , and when the states are extended the LDOS is correspondingly continuous. However, in an infinite system with localized states the DOS will remain continuous while the LDOS becomes discrete.^{14,17,18} This has been discussed more recently in the context of non-interacting electrons by a number of authors.^{19,20,21,22}

With this in mind, the geometric average of the density of states (GADOS)

$$\rho_g(\omega) = \left[\prod_{i=1}^N \rho(\mathbf{r}_i, \omega) \right]^{1/N}, \quad (1)$$

has been proposed^{6,7,8,9,21} as a possible order parameter of the Anderson localization transition. Note that if the LDOS at a given energy ω is zero on *any* site, the GADOS at that energy will be zero. Therefore, in an infinite system $\rho_g(0) \rightarrow 0$ signals a metal-insulator transition, where $\omega = 0$ corresponds to the Fermi level.

In this paper we explore some potential pitfalls in the use of this measure. Our central results are (1) that a finite energy resolution changes the scaling behavior of $\rho_g(\omega)$ and makes the determination of the mobility edges difficult and (2) that simply a decline, as opposed to a

zero, in the GADOS is not uniquely associated with the phenomenon of localization. We arrive at these conclusions in the context of a system of non-interacting electrons on a lattice with random potential values at each site (Section II A). First, we consider finite-size systems and use a standard numerical diagonalization approach (Section II B). In these systems, the density of states is discrete, but a spectrum similar to the thermodynamic result can be obtained by inserting a finite energy resolution, a process mathematically parallel to the presence of an inelastic scattering rate. We demonstrate (Section III A) some misinterpretations which may arise, we sketch the scaling procedures, explored in more detail elsewhere,^{21,23} which provide reliable phase information, and we examine in particular the influence of a finite energy resolution on the scaling behavior. Second, we treat the infinite system within the coherent potential approximation (CPA) (Section II C). This method is known to accurately reproduce the disorder-averaged DOS while not capturing the multiple-scattering processes responsible for Anderson localization. We find (Section III B) that the CPA GADOS declines with increasing disorder and suggest that this is due to small wavefunction amplitudes at sites of extreme potential. In summary, the dependence of $\rho_g(\omega)$ on disorder strength alone, in the absence of a clearly defined zero, is not a reliable measure of localization, and furthermore when the energy resolution is finite, scaling will be affected.

II. CALCULATIONS

A. Model

In this work, we will use a site-disordered model, in which the site energies ϵ_i take random values, while the hopping matrix element t is fixed. For the simplest case of spinless fermions, the Hamiltonian takes the form

$$H = \sum_i |i\rangle \epsilon_i \langle i| - t \sum_{\langle i,j \rangle} |i\rangle \langle j| \quad (2)$$

where $\langle i, j \rangle$ indicates nearest neighbour sites on the lattice, and $|i\rangle$ is a ket corresponding to the Wannier orbital attached to the i th site. In this work, we will present results for box-distributed disorder, where ϵ_i are uniformly distributed between $-W/2$ and $+W/2$, with probability distribution $P(\epsilon) = W^{-1} \Theta(W/2 - |\epsilon|)$ where Θ is a step function. We will consider two cases: the $d = 1$ chain where all states are known to be localized for any nonzero W ,²⁴ and the $d = 3$ cubic lattice for which all states are localized when $W = 16.5$.^{25,26}

We take two approaches to finding the electronic structure of the disordered lattice—exact numerical calculation and the coherent potential approximation—both of which are standard.

B. Exact numerical calculation (ENC)

The Hamiltonian given in Eq. (2) describes noninteracting Fermions, so that exact single-particle eigenstates may be found by numerically diagonalizing, using the LAPACK libraries, the matrix $H_{ij} = \epsilon_i \delta_{i,j} - t \delta_{\langle i,j \rangle}$, where $\delta_{\langle i,j \rangle}$ is one for nearest neighbor sites and zero otherwise. For a system with N sites, we obtain eigenvalues E_α ($\alpha = 1, \dots, N$) and corresponding eigenvectors $\Psi_\alpha(\mathbf{r}_i)$. We consider systems of linear size L (measured in units of the lattice constant) and dimension $d = 1$ or 3 , having $N = L^d$ lattice sites in total.

To calculate the GADOS using the numerical solution, the LDOS is obtained from the resulting eigenvectors:

$$\rho(\mathbf{r}_i, \omega) = \sum_\alpha |\Psi_\alpha(\mathbf{r}_i)|^2 \delta(\omega - E_\alpha). \quad (3)$$

In numerical calculations, where one has a discrete spectrum, one generally approximates the delta-function by bins of width γ :

$$\delta(\omega - E_\alpha) \approx \gamma^{-1} \Theta\left(\frac{\gamma}{2} - |\omega - E_\alpha|\right). \quad (4)$$

The LDOS approaches the thermodynamic result when $\gamma > \Delta_N(\omega)$ where $\Delta_N(\omega) = [\rho(\omega)L^d]^{-1} \sim 4dt/N$ is the energy level spacing due to the finite size of the system. This binning procedure is essentially equivalent to approximating

$$\rho(\mathbf{r}_i, \omega) \approx -\pi^{-1} \text{Im}G(\mathbf{r}_i, \mathbf{r}_i, \omega + i\gamma), \quad (5)$$

which is significant because it provides a point of reference between our results and results for many-body calculations of the single-particle Green's function.

The DOS is the arithmetic average of this: $\rho(\omega) = N^{-1} \sum_i \rho(\mathbf{r}_i, \omega)$, while the GADOS is as defined in Eq. (1). Representative examples of our results for the DOS and the GADOS in both one and three dimensions are shown in Fig. 1.

We present results both for $\gamma = 0$ and $\gamma \neq 0$. For $\gamma \neq 0$, we calculate the LDOS using Eq. (4). For $\gamma = 0$, we calculate the LDOS using Eq. (3) (a procedure which is only possible for noninteracting systems) in which case ρ_g is only nonzero for energies corresponding to an energy eigenvalue. This result is subsequently smoothed using a binning procedure. Note the key distinction that when $\gamma = 0$ the binning is done after the GADOS is calculated.

An important technical issue which must be discussed is disorder averaging. In order to improve the signal-to-noise ratio, we typically present results which have been averaged over several hundred impurity configurations. For $\rho(\omega)$ and for the IPR, this is a meaningful process. For $\rho_g(\omega)$ it is less clear whether one should take the arithmetic average or the geometric average, as was done in Ref. [27], of different samples. We have studied both averaging procedures and have determined that they yield similar results, except for small values of

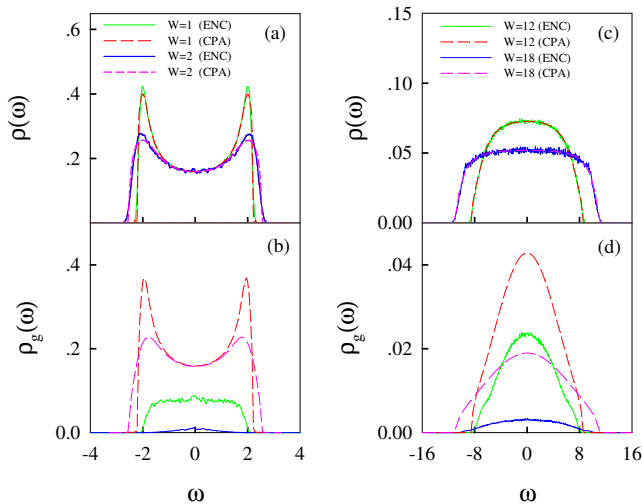


FIG. 1: (Color online) (a) $d = 1$ DOS; (b) $d = 1$ GADOS; (c) $d = 3$ DOS; and (d) $d = 3$ GADOS. In each case results from the ENC and from the CPA are shown for two values of disorder strength. The ENC results for $d = 1$ are for $N = 2000$ averaged over 400 samples, while those for $d = 3$ are for $L = 15$ averaged over 200 samples. All ENC results use $\gamma = 0.05$.

$\gamma \lesssim \Delta_N$, for which the geometric averaging becomes unreliable: If any particular disorder configuration fails to have an eigenvalue in a particular bin, then $\rho_g(\omega)$ vanishes for that bin. For this reason, we find that geometrically averaging disorder configurations for $\rho_g(\omega)$ exaggerates the already high sensitivity of the GADOS to single sites with high potential, and we have adopted the arithmetic average for calculating the disorder average of $\rho_g(\omega)$.

For purposes of comparison, it is also useful to calculate the IPR,^{14,16} which is known to be a reliable and sensitive measure of localization. For normalized eigenstates, the IPR for eigenstate α is

$$A_\alpha = \sum_i |\Psi_\alpha(\mathbf{r}_i)|^4 \quad (6)$$

and it is common to average the IPR over energy bins of width γ according to

$$A(\omega) = \frac{\sum_\alpha \Theta(\frac{\gamma}{2} - |E_\alpha - \omega|) A_\alpha}{\sum_\alpha \Theta(\frac{\gamma}{2} - |E_\alpha - \omega|)}. \quad (7)$$

It is the scaling of these quantities with system size which determines whether states are localized: For a system with N sites, both A_α and $A(\omega)$ scale as N^{-1} for extended states, but saturate at a finite value when the localization length ξ is less than the linear dimension L of the system. In practice when systems with $L > \xi$ are computationally inaccessible, localization can be inferred when $A(\omega)$ vs. N^{-1} extrapolates to a nonzero value.

C. Coherent potential approximation (CPA)

The CPA is the second approach we take to determine the electronic structure of our model. This is an effective medium theory, modelling a randomly distributed impurity potential ϵ_i with a self-energy $\Sigma(\omega)$. The self-consistent equation for the self-energy in the CPA is²⁸

$$0 = \int d\epsilon P(\epsilon) \frac{\epsilon - \Sigma(\omega)}{1 - (\epsilon - \Sigma(\omega))G_{loc}(\omega)} \quad (8)$$

where the on-site potential is distributed randomly according to the distribution $P(\epsilon)$, for which we use the box-distribution as described in Section II A. The disorder-averaged local Green's function is

$$G_{loc}(\omega) = \frac{1}{N} \sum_{\mathbf{k}} \frac{1}{\omega - t(\mathbf{k}) - \Sigma(\omega)} \quad (9)$$

where, for a tight-binding lattice

$$t(\mathbf{k}) = \begin{cases} -2t \cos k & d = 1 \\ -2t(\cos k_x + \cos k_y + \cos k_z) & d = 3 \end{cases}$$

is the dispersion of the lattice. Equation (8) is a statement that when averaged over the effective disorder potential $\epsilon - \Sigma$ the T-matrix vanishes.

We construct $\rho_g(\omega)$ from the CPA results using the following simple approach: We find the LDOS for a site embedded in an effective medium characterized by the CPA self-energy $\Sigma(\omega)$, where $\Sigma(\omega)$ is determined from Eq. (8). We call this LDOS $\rho_\epsilon(0, \omega)$ because the site is defined to sit at the origin and the site potential is ϵ . We then take the geometric average over an ensemble of systems where ϵ satisfies the same distribution function $P(\epsilon)$ used in the CPA calculation: $\ln[\rho_g^{CPA}(\omega)] = \int d\epsilon P(\epsilon) \ln[\rho_\epsilon(0, \omega)]$. Note that if we take the arithmetic average instead we simply recovered the CPA DOS, i.e. $\int d\epsilon P(\epsilon) \rho_\epsilon(0, \omega) = \rho^{CPA}(\omega) \equiv -\text{Im} G_{loc}(\omega)/\pi$.

Specifically, we solve the equations of motion for the Green's function with the site energy ϵ at the origin,

$$[\omega^+ - \epsilon]G(0, 0, \omega) - t \sum_n \delta_{\langle 0, n \rangle} G(\mathbf{r}_n, 0, \omega) = 1$$

$$[\omega^+ - \Sigma(\omega)]G(\mathbf{r}_i, \mathbf{r}_\ell, \omega) - t \sum_n \delta_{\langle i, n \rangle} G(\mathbf{r}_n, \mathbf{r}_\ell, \omega) = \delta_{i, \ell}$$

where the case $i = \ell = 0$ is excluded from the second equation and $\omega^+ = \omega + i0$. These give

$$G(0, 0, \omega) = [1 + G_{loc}(\omega)(\Sigma(\omega) - \epsilon)]^{-1} G_{loc}(\omega) \quad (10)$$

with $G_{loc}(\omega)$ defined in Eqn. (9). We remark that if one imposes the self-consistency condition $G_{loc}(\omega) = \int d\epsilon P(\epsilon) G(0, 0, \omega)$ then the procedure we have outlined is equivalent to the CPA. Noting that $\rho_\epsilon(0, \omega) = -\text{Im} G(0, 0, \omega)/\pi$, we then find the GADOS via

$$\ln \rho_g^{CPA}(\omega) = \int d\epsilon P(\epsilon) \ln \left[-\frac{1}{\pi} \text{Im} G(0, 0, \omega) \right]. \quad (11)$$

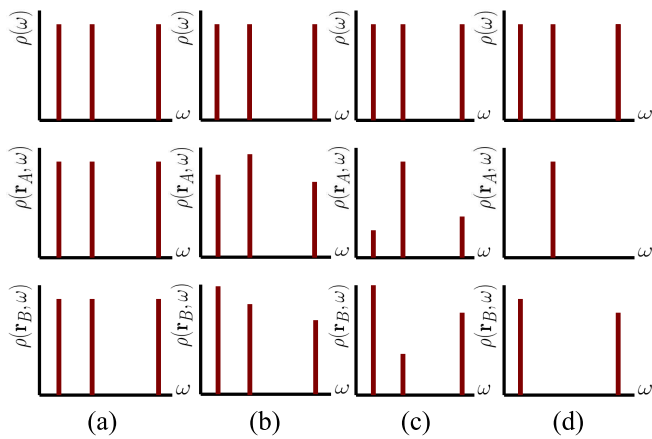


FIG. 2: (Color online) Sketches of the DOS and LDOS at two well-separated sites A and B in a sample of fixed size L with varying levels of disorder: (a) no disorder, (b) $W < W_c$, (c) $W > W_c$ but $\xi > L$, and (d) $W > W_c$ and $\xi \ll L$ and in particular $\xi \ll |\mathbf{r}_A - \mathbf{r}_B|$.

The CPA results for the $\rho(\omega)$ and $\rho_g(\omega)$ are compared with exact numerical results in Fig. 1. While the CPA reproduces the exact $\rho(\omega)$ accurately, there is a significant discrepancy between $\rho_g^{\text{CPA}}(\omega)$ and $\rho_g^{\text{ENC}}(\omega)$, presumably because the CPA does not capture the quantum interference to which the LDOS and hence GADOS are sensitive. Nonetheless, the CPA captures the general trend that $\rho_g(\omega)$ is a decreasing function of W . We will explore this point in more detail below (Section III B).

III. RESULTS AND DISCUSSION

A. Finite systems

We begin with our results on finite size systems in one and three dimensions. It may be useful to keep in mind three energy scales and three corresponding length scales. Δ_ξ is a measure of the average level spacing in the LDOS caused by localization. Larger values of Δ_ξ correspond to stronger localization and shorter localization length: $\Delta_\xi \sim 1/\xi^d$. Both ξ and Δ_ξ depend on ω . Δ_N is a measure of the mean level spacing in the DOS caused by the finite size of the system. Larger values of Δ_N correspond to smaller system sizes: $\Delta_N \sim 1/N = 1/L^d$. Finally, γ is the size of the energy bin width used in numerical calculations of the LDOS [Eq. (4)] and the IPR [Eq. (7)]. As suggested by Eq. (5), γ plays the same role as an inelastic scattering rate and the corresponding length scale is therefore an effective inelastic mean free path, $l_\gamma \sim 1/\gamma^{1/d}$.²⁹

Fig. 2 presents a useful framework for considering the effects of finite size on calculations of ρ_g . Four cartoons are presented corresponding to four values of disorder strength, all in a finite-size system of length L with $\gamma = 0$: (a) no disorder, (b) weak disorder such that no localiza-

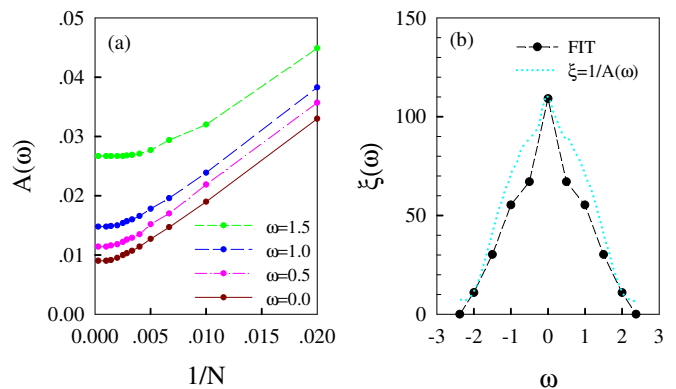


FIG. 3: (Color online) (a) The inverse participation ratio as a function of N^{-1} at four different energies for a $d = 1$ chain with $W = 1$ and $\gamma = 0.1$. (b) The localization length extracted by a fit to $A(\omega, N)$ (see text), and an alternative definition $A^{-1}(\omega, N_{max})$ of the localization length ($N_{max} = 2000$). The IPR is averaged over 400 disorder configurations for each value of N . Energies are measured in units of the hopping integral t .

tion takes place, (c) intermediate disorder such that localization occurs but with localization length large compared to the system size, and (d) strong disorder such that the localization length is much less than the system size. In each case a sketch is given within some frequency window of the DOS (for the whole system) and the LDOS at two well-separated sites A and B . The lengths of the lines correspond to the weights of the delta-function peaks in the DOS and LDOS at the discrete eigenenergies of the system. For a system with no disorder, case (a), the states will be not only extended but also, at low energies, fairly uniform so the weights of the eigenstates at a given site will be roughly the same. When disorder is introduced but no localization occurs, case (b), the weights at each site are shifted as sites become more and less energetically favorable. When localization begins but $\xi > L$, case (c), the unevenness of the weights in the LDOS simply becomes more pronounced. Only when localization is strong enough that $\xi \ll L$, case (d), do some of the weights become exponentially small.

Presenting our results, we begin with the case of a one dimensional chain, which is useful for several reasons. First, it is simple: there is no Anderson transition. All states are strongly localized for any nonzero W , with $\xi \approx \pi\ell$ where ℓ is the mean free path.^{1,24} Furthermore, the limits $L < \xi$ and $L > \xi$ are both accessible in numerical computations. Finally, the fact that we can study instances of localization with W less than the bandwidth allows us to distinguish two distinct factors which cause a decline in the GADOS—exponential tails of localized eigenstates and small wavefunction amplitudes at sites of extreme potential.

Fig. 3 demonstrates how the IPR shows localization in this $d = 1$ case. In Fig. 3 (a), there is a clear crossover from $A \sim 1/N$ to A roughly constant at

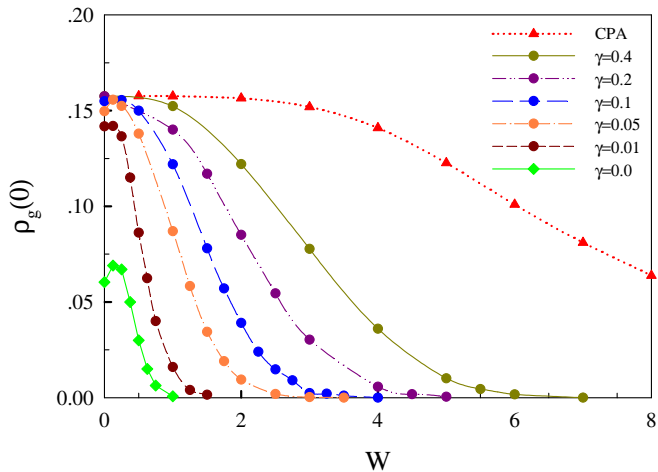


FIG. 4: (Color online) Dependence of the GADOS at $\omega = 0$ on W in one dimension, showing ENC results for several bin widths and CPA results. Calculations are in the strongly-localized regime $N = L = 2000 \gg \xi$ and the results are averaged over 400 disorder configurations. Energies are measured in units of the hopping integral t .

$L = \xi$. The corresponding energy-dependent localization lengths are shown in Fig. 3 (b). The localization lengths have been extracted by fitting the IPR to a form $A(\omega, N) = A(\omega, \infty) \coth(N/2\xi)$ which we expect for one-dimensional wavefunctions that are decaying exponentially over a length scale ξ with periodic boundary conditions. Because $A(\omega, N)$ saturates for $L \gg \xi$, $A(\omega, \infty) \approx A(\omega, N_{max})$, where $N_{max} = 2000$. The values of $\xi(\omega)$ determined in this way are quantitatively consistent with earlier calculations,³⁰ and are also close to the quantity $A^{-1}(\omega, \infty)$ that is frequently taken as a definition of the localization length. The quantitative differences between the two definitions are not important for this work. Rather, the main point of Fig. 3 is to establish that the $d = 1$ results presented below are for the strongly-localized regime $L \gg \xi$, where we expect $\rho_g(\omega)$ to be strongly influenced by the exponential tails of the wavefunctions.

Fig. 4 shows the variation of the GADOS at the band center as a function of disorder strength for a finite size system. Results from the ENC are shown for several values of the energy bin widths including $\gamma = 0$, and the CPA result is also shown. Naïvely, there appears to be an Anderson transition at nonzero W . If it were to be assumed that the Anderson transition occurs when $\rho_g(\omega) = \eta\rho(\omega)$ with $\eta \ll 1$, then $\rho_g(\omega)$ erroneously predicts an Anderson transition at a *nonzero* critical disorder W_c^{eff} , where W_c^{eff} is strongly γ dependent. This happens for two reasons: First, when $\gamma > \Delta_\xi$, the discrete nature of the LDOS is hidden, and moreover when $L < \xi$ even exponentially localized states have significant amplitude at all sites. The resulting potential for errors points both to the importance of performing a proper scaling analysis and also to the significance of γ in the scaling, a feature

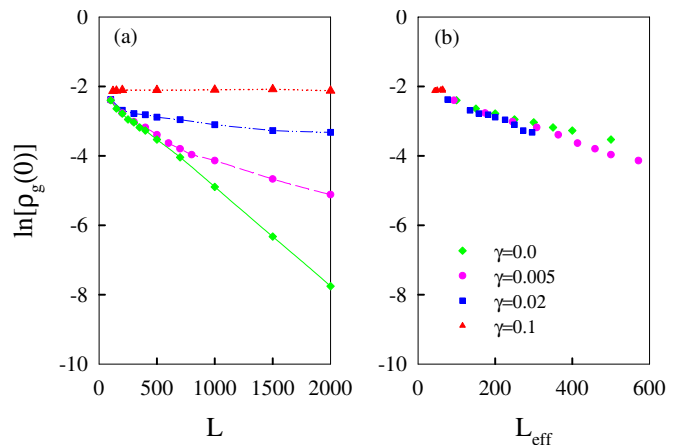


FIG. 5: (Color online) (a) The scaling with chain length of the ENC GADOS at the band center in one dimension with $W = 1$ for several bin widths including zero. Results are averaged over 400 disorder configurations. (b) The same data as in (a), plotted against L_{eff} .

key to the applicability of this method in many-body calculations.

We remark that the γ dependence of $\rho_g(\omega)$ at small values of W in Fig. 4 is a finite size effect due to the varying number of discrete states which fall in each energy bin [see Eq. (4)]. This issue does not arise when W is large because in this case the eigenvalues shift significantly from one disorder configuration to the next and hence the number which fall in any given energy bin is stabilized by sample averaging. Equivalently, finite size effects appear for small W because the mean free path is larger than the system size.

In Fig. 5, we examine the scaling behavior of $\rho_g(\omega)$. Ref. [21] has done a detailed scaling analysis of the critical regime $L < \xi$ for the case $\gamma = 0$, i.e. where individual wavefunctions are studied. Our goal is to study the influence of a finite energy resolution, a necessary feature of a number of many-body approaches, on the scaling behavior. Figure 5(a) shows the scaling of $\rho_g(0)$ with chain length for $W = 1$ and several values of γ including zero. At this disorder strength, $\xi(0) \approx 120$ lattice spacings and $\Delta_\xi(0) \approx 0.05t$. For $\gamma = 0$ and $L > \xi$, as the system size increases the exponentially decaying form of the localized states manifests itself, and $\rho_g(0) \sim \rho(0) \exp(-L/2\xi)$. (This form is derived using periodic boundary conditions). For $\gamma = 0$ and $L < \xi$, the system is in a critical regime where the decline has a power law rather than exponential form;²¹ however the difference is difficult to distinguish over this short scale. For nonzero γ , ρ_g scales exponentially for $L < \ell_\gamma$ but saturates at larger values of L . We make the ansatz that there is an effective system size dominated by the shorter of the two relevant lengths:

$$L_{eff} = (1/L + 1/\ell_\gamma)^{-1}, \quad (12)$$

where $\ell_\gamma = (\rho\gamma)^{1/d}$, such that $\rho_g(0) \sim$

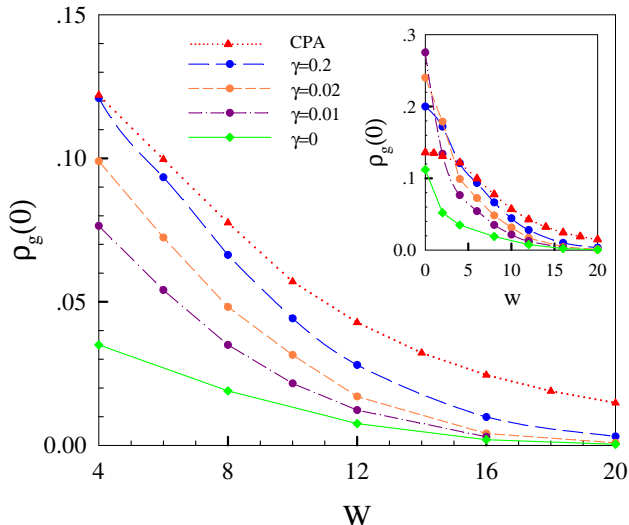


FIG. 6: (Color online) Dependence of the GADOS at the band center on W (in units of t) in three dimensions showing ENC results for several bin widths and CPA results. Inset includes results for weak disorder where there is a strong γ dependence. $L = 15$, $N = L^3$ and the results are averaged over 200 disorder configurations.

$\rho(0) \exp(-L_{\text{eff}}/2\xi)$. In Fig. 5(b), a plot of the data from Fig. 5(a) versus L_{eff} shows that the ansatz works well. One immediate consequence of Eq. (12) is that when $L \gg \ell_\gamma$, $\rho_g(0)$ saturates at $\sim \rho(0) \exp(-\ell_\gamma/2\xi)$. Thus, in Fig. 4, the apparent critical disorder W_c^{eff} actually marks the crossover from $\xi > \ell_\gamma$ to $\xi < \ell_\gamma$ rather than a localization transition. We conclude that the scaling of $\rho_g(\omega)$ with N can be used to place an upper bound on the disorder strength at which localization occurs: If an exponential decay of $\rho_g(0)$ with increasing N is seen, then localization is occurring. However, if γ is too large, the effect will be masked. Essentially this analysis may lead to false negatives but not to false positives, and in particular the true result is approached as $\gamma \rightarrow 0$.

We turn our attention now to the $d = 3$ cube with $N = L^3$ sites, and $L \leq 20$. This case differs from $d = 1$ in two important ways. First, there is known to be an Anderson transition which, for $\omega = 0$ occurs at $W_c = 16.5t$. Second, unless W is very large, we are generally restricted to $L \ll \xi$.

Consider first the variation of the GADOS at the band center as a function of disorder strength, Fig. 6. As in the $d = 1$ case, the ENC results are γ dependent, increasing with increasing γ . Unlike in the $d = 1$ case, they are similar to the CPA result, a point discussed further in Section III B. The weak disorder results are included in the inset and show strong γ dependence for the same reasons discussed in the $d = 1$ case.

Again, the correct approach is a scaling analysis. Fig. 7 (a) shows the logarithm of the GADOS versus the system size L ($N = L^3$) using $\gamma = 0$, and Fig. 7 (b) shows

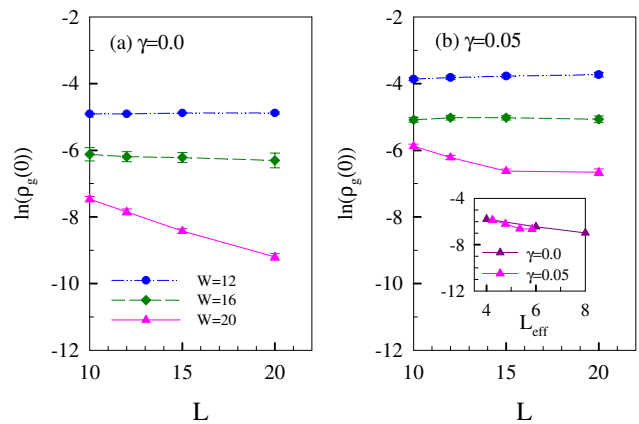


FIG. 7: (Color online) The scaling with system size of the ENC GADOS at the band center in three dimensions, showing disorder strengths above and below the localization transition, $W_c = 16.5$. (a) $\gamma = 0$ and (b) $\gamma = 0.05$. The inset shows the scaling with L_{eff} for $W = 20$. Results are averaged over 200 disorder configurations. Energies are measured in units of the hopping integral t .

the same quantity for a nonzero energy bin width. From these plots it is easy to distinguish localized from delocalized behavior, at least outside of the critical regime $L < \xi$. In the delocalized phase, there is no significant variation with system size. This is consistent with the log-normal distribution of the LDOS predicted by Mirlin,^{20,23} and furthermore the decline in the value of $\rho_g(0)$ with increasing W is consistent with a decrease in the position of the maximum of the distribution as the transition is approached, also predicted by Mirlin.^{20,23} In the localized phase, the exponential decay as well as the saturation for $\gamma \neq 0$ are similar to what is seen in one dimension. The larger error bars on the $\gamma = 0$, $W = 16$ results are related to the proximity to the transition: The mobility edges are very close to $\omega = 0$ and hence the energy window used in generating $\rho_g^{\gamma=0}(0)$ must be especially narrow to avoid including localized states outside the mobility edge. The reduction in the number of states included leads to noisier results.

In one dimension, we showed that the strong dependence of $\rho_g(\omega)$ on γ can be understood in terms of an effective length L_{eff} . We find this to be true for $d = 3$ as well. The inset to Fig. 7(b) shows that for the strongly-localized phase ($W = 20$), the data for $\gamma = 0$ and $\gamma = 0.05$ collapse onto a single curve when plotted against L_{eff} [Eq. (12)]. We remark that for $\gamma = 0.05$, $\ell_\gamma \approx 8$ lattice constants. Since $L_{\text{eff}} < \ell_\gamma$, this means that even for a large range of L , the effective range sampled by scaling is quite small. In particular, if this re-scaling of lengths applies to the critical regime, this implies that the determination of the mobility edges by scaling analysis may be severely limited in, for example, many-body calculations which are performed at complex frequencies $\omega + i\gamma$.

Finally, Fig. 8 compares three phase diagrams for $d = 3$. First, we have shown published³¹ results for the

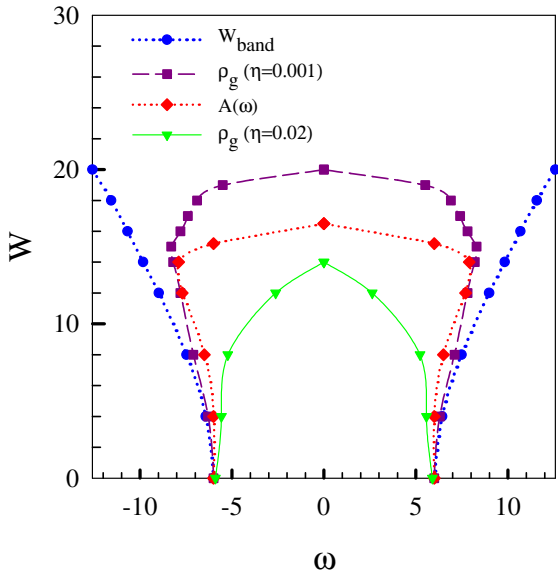


FIG. 8: (Color online) The bandwidth W_{band} and the mobility edges $\omega_{c\pm}$ in three dimensions, with the latter estimated using the scaling of the IPR and $\rho_g(\omega) < \eta\rho(\omega)$ for two values of η . Further details provided in the text.

mobility edges based on the scaling of the IPR as a standard of comparison. The second method used is to call states at a given energy localized when the curve of $\rho_g(\omega)$ versus W , like that in Fig. 6, drops below some cutoff $\rho_g(\omega) = \eta\rho(\omega)$. (System size $L = 15$ was used, averaged over 100 to 200 samples, with $\gamma = 0.05$.) We show curves using two values of η : one which results in a localization transition at smaller W than the IPR transition, and another which results in a localization transition at higher disorder strength than the IPR transition. The scaling of $\rho_g(\omega)$ with system size could also be used to produce a phase diagram, and the transition would always lie on the high W side of the IPR line, with the two coinciding in the limit $\gamma \rightarrow 0$. However, the construction of such a diagram is similarly computationally intensive to the equivalent IPR calculation and in an interacting system offers no obvious advantages.

B. Infinite systems

We now turn our attention to infinite systems. Recent DMFT work^{6,7,8,9} includes plots similar to those in

Fig. 6, showing the GADOS declining as a function of W . Here, we point out that factors other than exponentially decaying tails of localized states may lead to a decline (although not a zero) in the GADOS.

The GADOS is very sensitive to small values of the LDOS on individual sites. Small values may occur due to localization, but they may also occur due to the reduction in amplitude of extended wavefunctions at sites where the magnitude of the potential is large. The CPA is a convenient tool for examining this issue because it is known to include the latter effect but not the former. We show the CPA results for $\rho_g(0)$ as a function of W for $d = 1$ in Fig. 4 and for $d = 3$ in Fig. 6. In both cases $\rho_g^{CPA}(0)$ declines at large W . In the $d = 1$ case, the fact that $\rho_g^{CPA}(0)$ is roughly constant over the range $0 < W < 4$ suggests that the suppression of ρ_g in the ENC calculations is due primarily to the exponentially decaying tails of the localized eigenstates. For $d = 3$ the decline in $\rho_g^{CPA}(0)$ is especially steep and fairly close to the ENC results, suggesting that in contrast to the $d = 1$ case the W dependence of $\rho_g(\omega)$ is dominated by lattice sites with extreme potential, rather than by exponential tails of localized eigenstates. Therefore, even in an infinite system, a decline in $\rho_g(\omega)$ with increasing W does not necessarily imply the approach to a localization transition. This does not appear to change the central conclusions of Refs. 6,7,8,9, which are based on zeros in the GADOS.

IV. CONCLUSIONS

In summary, for finite-size systems we have demonstrated some of the false conclusions which may be drawn if a scaling analysis is not used and shown how the use of a finite energy resolution will influence the scaling. Moreover, in infinite systems we have demonstrated that the GADOS can decline as a function of disorder strength without localization occurring.

Acknowledgments

We wish to thank Ilya Vekhter for helpful conversations. We would also like to acknowledge support by NSERC and by Trent University.

¹ P. A. Lee and T. Ramakrishnan, *Reviews of Modern Physics* **57**, 287 (1985).

² P. Anderson, *Physical Review* **109**, 1492 (1958).

³ D. Belitz and T. Kirkpatrick, *Reviews of Modern Physics* **66**, 261 (1994).

⁴ E. Abrahams, S. V. Kravchenko, and M. P. Sarachik, *Reviews of Modern Physics* **73**, 251 (2001).

⁵ V. Dobrosavljevic and G. Kotliar, *Physical Review B* **50**, 1430 (1994).

⁶ V. Dobrosavljevic and G. Kotliar, *Physical Review Letters*

- 78**, 3943 (1997).
- ⁷ M. Aguiar, E. Miranda, and V. Dobrosavljevic, *Physical Review B* **68**, 125104 (2003).
 - ⁸ V. Dobrosavljevic, A. Pastor, and B. Nikolic, *Europhysics Letters* **62**, 76 (2003).
 - ⁹ K. Byczuk, W. Hofstetter, and D. Vollhardt, *Physical Review Letters* **94**, 056404 (2005).
 - ¹⁰ E. Miranda and V. Dobrosavljevic, *Reports on Progress in Physics* **68**, 2337 (2005).
 - ¹¹ M. Aguiar, V. Dobrosavljevic, E. Abrahams, and G. Kotliar, *Physical Review B* **73**, 115117 (2006).
 - ¹² A. Georges, G. Kotliar, W. Krauth, and M. J. Rozenberg, *Reviews of Modern Physics* **68**, 13 (1996).
 - ¹³ J. Edwards and D. Thouless, *Journal of Physics C: Solid State Physics* **5**, 807 (1972).
 - ¹⁴ D. Thouless, *Physics Reports* **13**, 93 (1974).
 - ¹⁵ E. Hofstetter and M. Schreiber, *Physical Review B* **48**, 16979 (1993).
 - ¹⁶ R. Bell and P. Dean, *Discussions of the Faraday Society* **50**, 55 (1970).
 - ¹⁷ D. Thouless, *Journal of Physics C: Solid State Physics* **3**, 1559 (1970).
 - ¹⁸ R. Abou-Chacra, P. Anderson, and D. Thouless, *Journal of Physics C: Solid State Physics* **6**, 1734 (1973).
 - ¹⁹ A. Mirlin and Y. Fyodorov, *Nuclear Physics B* **366**, 507 (1991).
 - ²⁰ A. Mirlin and Y. Fyodorov, *Physical Review Letters* **72**, 526 (1994).
 - ²¹ M. Janssen, *Physics Reports* **295**, 1 (1998).
 - ²² J. Brndiar and P. Markoš, *Physical Review B* **74**, 153103 (2006).
 - ²³ A. D. Mirlin, *Physics Reports* **326**, 259 (2000).
 - ²⁴ A. Gogolin, *Physics Reports* **86**, 1 (1982).
 - ²⁵ A. MacKinnon and B. Kramer, *Physical Review Letters* **47**, 1546 (1981).
 - ²⁶ H. Grussbach and M. Schreiber, *Physical Review B* **51**, 663 (1995).
 - ²⁷ G. Schubert, A. Weisse, and H. Fehske, *Physical Review B* **71**, 045126 (2005).
 - ²⁸ L. Schwartz, F. Brouers, A. Vedyayev, and H. Ehrenreich, *Physical Review B* **4**, 3383 (1971).
 - ²⁹ Strictly speaking, it is the dephasing rate which determines the length cutoff, as discussed in Ref. [32]. For our qualitative discussion, however, the distinction is not important.
 - ³⁰ G. Casati, I. Guarneri, F. Izrailev, S. Fishman, and L. Molinari, *J. Phys. Condens. Matter* **4**, 149 (1992).
 - ³¹ B. R. Bulka, B. Kramer, and A. MacKinnon, *Zeitschrift für Physik B, Condensed Matter* **60**, 13 (1985).
 - ³² B. Altshuler and A. Aranov, *Solid State Communications* **30**, 115 (1979).